Anomalous Size-Dependent Decay of Low-Energy Luminescence from PbS Quantum Dots in Colloidal Solution

ARTICLE *in* ACS NANO · SEPTEMBER 2012

Impact Factor: 12.88 · DOI: 10.1021/nn3029106 · Source: PubMed

8 AUTHORS, INCLUDING:

P. S. Parfenov
ITMO University
27 PUBLICATIONS **129** CITATIONS
SEE PROFILE

A. V. Fedorov
ITMO University
189 PUBLICATIONS **1,040** CITATIONS
SEE PROFILE

Mikhail Artemyev
Belarusian State University
188 PUBLICATIONS **3,667** CITATIONS
SEE PROFILE

A. V. Baranov
ITMO University
270 PUBLICATIONS **1,946** CITATIONS
SEE PROFILE

Anomalous Size-Dependent Decay of Low-Energy Luminescence from PbS Quantum Dots in Colloidal Solution

Elena V. Ushakova,[†] Aleksandr P. Litvin,[†] Peter S. Parfenov,[†] Anatoly V. Fedorov,[†] Mikhail Artemyev,[‡] Anatoly V. Prudnikau,[‡] Ivan D. Rukhlenko,[§] and Alexander V. Baranov[†,*]

[†]National Research University of Informational Technologies, Mechanics and Optics, 197101 Saint Petersburg, Russia, [‡]Institute for Physico-Chemical Problems, Belarusian State University, 220080 Minsk, Belarus, and [§]Advanced Computing and Simulation Laboratory (AχL), Department of Electrical and Computer Systems Engineering, Faculty of Engineering, Monash University, Clayton 3800, Victoria, Australia

ABSTRACT We report on an anomalous size dependence of the room-temperature photoluminescence decay time from the lowest-energy state of PbS quantum dots in colloidal solution, which was found using the transient luminescence spectroscopy. The observed 10-fold reduction in the decay time (from ~2.5 to 0.25 μs) with the increase in the quantum dots' diameter is explained by the existence of phonon-induced transitions between the in-gap state—whose energy drastically depends on the diameter—and the fundamental state of the quantum dots.

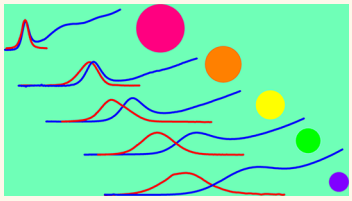

KEYWORDS: PbS quantum dots · near-infrared · size dependence · in-gap electronic state · quantum transition dynamics · photoluminescence decay · phonon-induced transitions

Colloidal nanocrystals quantum dots (QDs) made of narrow-bandgap IV–VI semiconductors, such as PbS and PbSe, have been the subject of much scholarly research due to being capable of effectively absorbing and emitting light and possessing size-tunable bands in the near-infrared (NIR) region.[1−3] These unique optical properties make colloidal QDs very attractive for applications in a variety of different areas—ranging from biology and medicine[4,5] to optoelectronics—including effective infrared photodetectors,[6] organic light-emitting diodes,[7,8] and photovoltaic devices, as well as solar cell technology.[9−11] Also of significance, from a practical viewpoint, is the large exciton Bohr radius and the almost identical effective masses of electrons and holes,[12] owing to which even QDs of relatively large sizes (4–10 nm) feature strong quantum confinement[13,14] and fundamental transitions in the 1–2 μm spectral range.

The dependence of energy of the lowest-energy electronic state on the QD's size and the associated peculiarities of the charge-carrier dynamics are of primary importance for applications and therefore have been intensively studied in the past decade.[15−24] It has been found that colloidal lead chalcogenide QDs possess some unconventional properties, such as the large, confinement-dependent Stokes shift[16,17,19,20,22,23] and the extraordinarily long photoluminescence (PL) lifetime in the microsecond range.[5,16,17,19,25,26] The variation in the Stokes shift's magnitude from several hundreds to tens of millielectronvolts, which occurs upon the increase in the QD's size from 2.5 to about 6 nm, have been reported in the earlier studies on colloidal QDs made of PbS.[19,20,22,23] This data, together with the experiments on infrared photoinduced absorption by PbS QDs,[22,23] indicates the existence of an electronic state whose energy within the QD's bandgap depends on the extent of the quantum confinement. The photoexcited electrons first relax to this state from the lowest conduction state nonradiatively, and then radiatively recombine, giving rise to the PL with a quantum yield of up to 70% at room temperature.[20] The origin of the emitting state with the size-dependent energy is still an issue of great scientific dispute.[20−23,27,28] In particular, a dark-exciton state,[24] a hybrid state consisting of a trapped electron and hole in the conduction band,[20] a trapped exciton state,[23] an exciton state split off due to the intervalley interaction,[29] and shallow-trap surface states[30] have all been considered as possible candidates for the unusually emitting state.

The PL lifetimes ranging from 1 to 2.7 μs have been reported for PbS QDs dispersed in organic solvents,[5,19,25,26] embedded in polymer films,[26,31,32] and arranged in closely packed ensembles.[20,22,23,32] A single-exponential PL

* Address correspondence to a_v_baranov@yahoo.com.

Received for review June 29, 2012 and accepted September 12, 2012.

Published online September 12, 2012
10.1021/nn3029106

decay was observed in most of these experiments, although a biexponential decay (with the fast component of 100 ns and the long component of 2.4 μs) was reported for the QDs of 3 nm in diameter, dispersed in tetrachloroethylene.[5] The relatively long PL lifetime for colloidal PbS QDs emitting in the NIR region (as compared to *e.g.*, CdSe QDs) is usually attributed to the decreased radiative recombination rate due to both the relatively low transition energy[33] and the effect of dielectric screening.[17] The first reason leads to the rise in the PL lifetime with the QD size. The corresponding calculations give a radiative lifetime of about 9 and 20 ns for PbS QDs with diameters of 3 and 8 nm, respectively. The effect of dielectric screening is the reduction of the field inside a sphere that has a high refractive index, and the associated increase of the PL lifetime by the factor $(\varepsilon_1 + 2\varepsilon_0)^2/(3\varepsilon_0)^2$, where ε_0 and ε_1 are the permittivities of the solvent host and the QD. Simple estimations show that the PL lifetime should increase by a factor of 11 for PbS QDs ($\varepsilon_1 = 17.2$)[12] in tetrachloromethane ($\varepsilon_0 = 2.2$),[34] and constitute about 100 and 220 ns for the QDs with diameters of 3 and 8 nm. These theoretical values are typically an order of magnitude smaller than the lifetimes that are measured experimentally. The reason for this is currently unclear. It is quite probable, however, that the high magnitude and strong size dependence of the PL lifetime are closely related to the size-dependent properties of the electronic state within the QD's bandgap whose decay gives rise to the PL. Unfortunately, only scattered data on the PL lifetime in semiconductor nanocrystals with diameters below 4.5 nm (emission wavelengths above 1250 nm) is available in the literature, especially for QDs in diluted solutions where their mutual interaction does not affect the PL kinetics.

In this paper, by employing the steady-state and transient photoluminescence spectroscopy, we comprehensively investigate the size dependency of the low-energy-PL lifetime for PbS QDs dispersed in tetrachloromethane (TCM). The correlation between this dependency and the characteristics of the in-gap electronic state was analyzed in a broad range of QD sizes from 2.5 to 8.8 nm. A 10-fold reduction (from ~2.5 to 0.25 μs) in the lowest-energy luminescence decay time with the QD size was observed and explained in terms of the size-dependent phonon-induced transitions from the in-gap state to the fundamental state of the QDs. The experiments were performed at a low concentration of nanocrystals in liquid solution at room temperature, to reduce as strongly as possible the influence of interactions between QDs themselves and between QDs and their environment on the dynamics of electronic transitions. The obtained room-temperature data are of particular interest due to possible applications of PbS QDs in optoelectronic devices operating at regular service conditions.

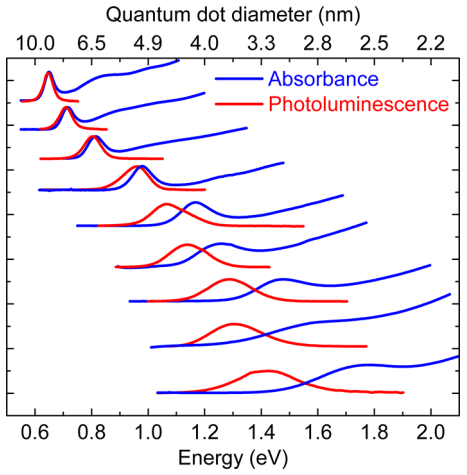

Figure 1. Absorption (blue curves) and PL (red curves) spectra of PbS-QDs/TCM at room temperature. The upper axis shows the QD diameters calculated from eq 5 using bandgap energies, which are determined by the lowest-energy absorption peaks.

RESULTS AND DISCUSSION

Absorption and Steady-State Luminescence Analysis. Figure 1 shows the typical absorption and PL spectra for different samples of PbS QDs in TCM (PbS-QDs/TCM) with mean diameters D ranging from 2.3 to 8.8 nm. The spectra demonstrate the size-dependent Stokes shift, which is a characteristic feature of PbS QDs. The values of this shift agree well with the previously reported data[19−22] for similar QDs with absorption band energy exceeding 1.3 eV. The shift, calculated as a difference between the energy of the absorption band and the energy of the luminescence band maximum, is shown in Figure 2a by solid squares.

A detailed analysis of the luminescence bands reveals that they consist of two components, the relative intensity of which depends on the mean size of the QDs. For the relatively large or relatively small QDs, the PL bands may be well fitted by a single Gaussian, whereas in order to fit the PL bands of QDs with diameters ranging from 3.5 to 6 nm (and bandgaps between 1.3 and 0.8 eV) two Gaussians are needed. Figure 2b illustrates this fact by the examples of QDs with the largest, smallest, and intermediate diameters. One can see that the high-energy PL component (PL1) exhibits a Stokes shift of about 4−5 meV, which is almost independent of the QD size. This component dominates the PL spectra of large QDs, but becomes almost undetectable for QDs with $D <$ 3.5 nm due to the drastic decrease of its intensity with the QD size. The low-energy PL component (PL2) features a size-dependent Stokes shift, while its intensity increases with the reduction of the QD size. It dominates the PL spectra of large QDs and disappears in the PL spectra of small ones. The open circles in Figure 2a show how the Stokes shift of component PL2 varies with the QD size and the bandgap

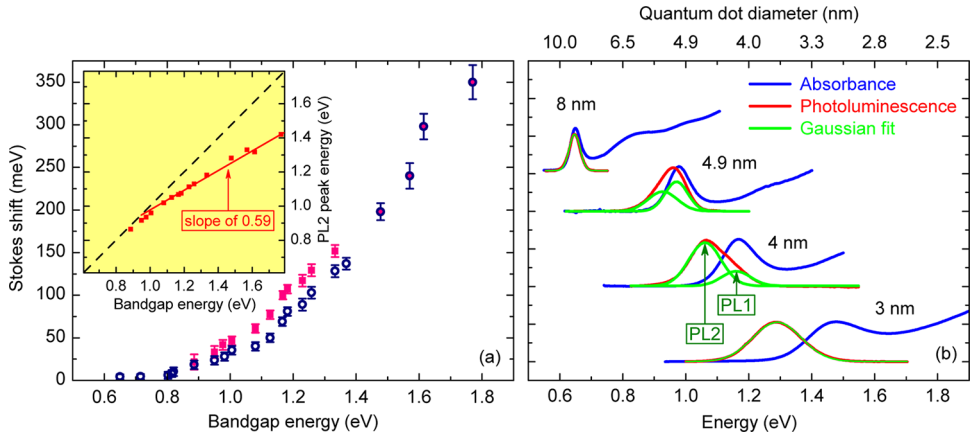

Figure 2. (a) Stokes shift of PL as a function of the QDs' bandgap energy. Solid squares show the energy shift of the absorption peak with respect to the PL band maximum, while open circles show the shift between the absorption peak and the PL2 peak. PL2 peak energy grows linearly with the QDs' bandgap energy, as shown by the solid line (of slope 0.59) in the inset of panel a. For reference, the dashed line with unity slope shows the energy of the absorption peak. (b) Representative set of PL bands for QDs of largest (~8 nm), smallest (~3 nm), and intermediate (4 and 4.9 nm) diameters. An asymmetry of the PL bands is seen for the QDs of intermediate sizes. These bands are well fitted by two Gaussians, while the PL bands of the QDs with diameters 8 and 3 nm may be fitted by a single Gaussian.

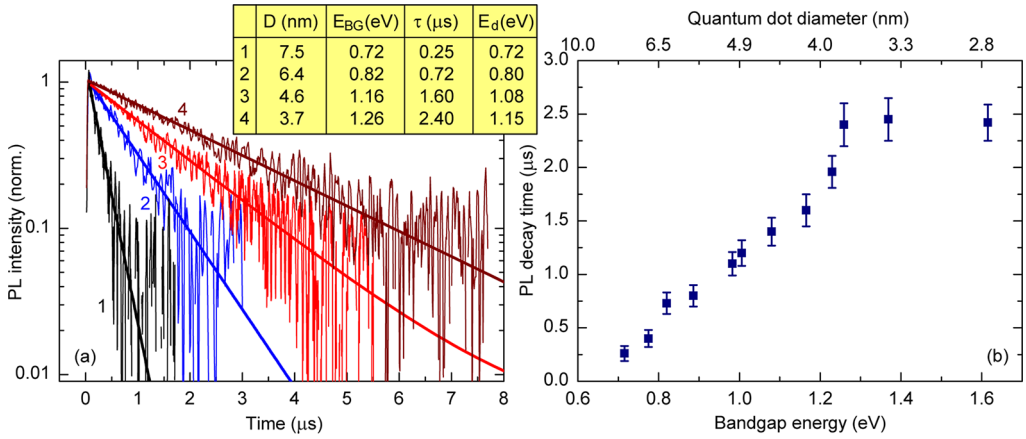

Figure 3. Decay of room-temperature PL from PbS-QDs/TCM. (a) PL decay curves for QD ensembles with mean diameters of 3.7, 4.6, 6.4, and 7.5 nm. Solid curves show single-exponential fittings. The legend shows bandgap energies (E_{BG}), detection energies (E_d), and the corresponding time constants (τ). (b) PL decay time as a function of the QDs' bandgap energy (bottom axis) and diameter (top axis). The error bars represent the standard deviations of 4–5 independent measurements.

(absorption peak) energy. The inset in Figure 2a demonstrates the dependencies of the absorption peak energy (dashed line) and the peak energy of the component PL2 (solid line) on the QDs' bandgap E_{BG}. A linear dependence of the PL2 peak energy on E_{BG}, with a slope of 0.59, is observed for E_{BG} exceeding 1 eV. Hence, the dependence of the peak energy of the PL2 component on the QDs' size is almost twice as weak as the similar dependence of E_{BG}.

Transient Photoluminescence Spectroscopy. We measured the PL decay at room temperature for the samples of QDs with diameters from 2.8 to 7.5 nm, which emit in the spectral range of 0.87–1.72 μm (1.42–0.72 eV). The total signal of PL1 and PL2 components was detected. Figure 3a shows the typical decay curves for QD ensembles with D = 3.7, 4.6, 6.4, and 7.5 nm. All the curves can be fit sufficiently well by a single exponential with the time constant between 0.25 and 2.5 μs. It should be noted that for QDs with diameters exceeding 6 nm, the PL decay features a more or less pronounced fast component, which cannot be resolved in our experiments and can be seen in Figure 3b as 30–40-ns spikes. The experimentally obtained dependence of the PL decay time on the QDs' bandgap energy (QDs' mean diameter) is shown in Figure 3b. The error bars represent the standard deviations calculated for 4–5 independent measurements. For QDs with mean diameters smaller than 4.4 nm, the microsecond-scale decay times of 2–2.5 μs (weakly depending on the mean diameters) were found.

These decay times agree well with those reported earlier for PbS QDs of similar sizes.[5,19,25,26] At the same time, an order-of-magnitude monotonic reduction of the PL decay time (down to 250 ns) has been observed upon increasing the QDs' diameter from 4 to 7.4 nm.

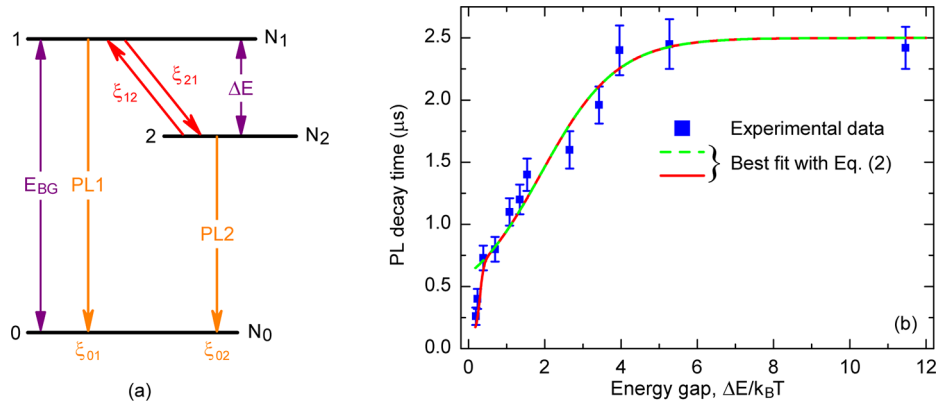

Figure 4. (a) Scheme of low-energy electronic states of PbS QDs with bandgap energy E_{BG}. The numbers 0, 1, and 2 denote ground, first excited, and "in-gap" energy states with populations N_0, N_1, and N_2; ξ_{ij} is the characteristic rate of transitions $j \rightarrow i$; ΔE is the energy gap between states 1 and 2. (b) PL decay time as a function of the energy gap ΔE between states 1 and 2 (in the units of k_BT). Experimental data is shown by solid squares. The error bars represent the standard deviations of 4−5 independent measurements. The dotted green curve is the best fit of the experimental data by eq 2. The red curve shows the result of fitting by eq 2, which takes into account the dependency $\xi_{01}(\Delta E)$ due to the acoustic-phonon relaxation.

To the best of our knowledge, such a dependency has never been reported before for the lowest-energy luminescence from the QDs made of other semiconductors. We believe that it may be explained by the peculiarities of the electronic energy structure of PbS QDs, namely, by the presence of the electron state with a confinement-dependent energy within the QDs' bandgap.

THEORETICAL ANALYSIS AND DISCUSSION

We now interpret the obtained data using a simple, three-level model of the low-energy electronic structure of PbS QDs, which was initially proposed by a number of authors.[19−22] The energy level diagram illustrating the model is shown in Figure 4a, where the numbers denote the ground state (0), the conventional lowest-energy electronic state of the QDs (1), and the "in-gap" electronic state (2). States 1 and 2 are separated by a size-dependent energy gap ΔE and have populations N_1 and N_2. The acronyms PL1 and PL2 denote the 1−0 and 2−0 optical transitions. The size-independent Stokes shift PL1 of 4−5 meV comes, most likely, from the PL phonon sideband, while the size-dependent Stokes shift PL2 (Δ_S) arises from the energy gap, that is, $\Delta_S = \Delta E$. The in-gap state is populated by nonradiative transitions from state 1, at the rate ξ_{21} that is supposed to be much larger than the recombination rate $\xi_{01} = \xi_{01}^{r} + \xi_{01}^{nr}$ of state 1 (here ξ_{01}^{r} and ξ_{01}^{nr} are the radiative and nonradiative recombination rates). The recombination rate ξ_{02} of state 2 is expected to be much smaller than ξ_{01}, thus leading to the microsecond-scale decay times of the lowest-energy luminescence from the QDs. The population transfer from state 2 to state 1 is possible at the rate $\xi_{12} = \xi_{21} \exp[-\Delta E/(k_BT)]$, where k_B is the Boltzmann constant and T is the temperature of the sample.

It is qualitatively clear that for $\Delta E \gg k_BT$ and $\xi_{21} \gg \xi_{01}, \xi_{02}$, the QD emission is dominated by the decay of the in-gap state, giving rise to component PL2 with the decay time $\tau = 1/\xi_{02}$. In sharp contrast to this, if $\Delta E \ll k_BT$ and the population transfer rate ξ_{12} is much larger than ξ_{02}, then the PL spectrum is dominated by recombination at the electron state 1. In the intermediate case, it is reasonable to expect that both components (PL1 and PL2) will be present in the PL spectrum. The proposed scenario is similar in some way to those used for the description of the temperature-induced electronic transitions in the systems with electronic sates separated by a fixed energy gap ΔE, which is comparable to k_BT. In the case of PbS QDs, and perhaps PbSe QDs, the energy gap may be tuned in a broad range at almost any temperature, owing to its strong dependency on the QD size.

To analyze the obtained experimental data in more detail, the dynamics of electronic transitions in the three-level system [see Figure 4a] was described using Pauli equations for the populations of the system's states.[35] Let us first consider the quasi-state luminescence spectra of the QDs. In the framework of the proposed model, the signals of the quasi-state luminescence at the maxima of the bands PL1 and PL2 are found to be

$$S_{PL1} = \frac{W_{n,0}}{\gamma_{nn}} \frac{|V_{0,1}|^2 \xi_{1n} \gamma_{22}}{\hbar^2 \xi_{01} \gamma_+ \gamma_-}, \quad S_{PL2} = \frac{W_{n,0}}{\gamma_{nn}} \frac{|V_{0,2}|^2 \xi_{1n} \xi_{21}}{\hbar^2 \xi_{02} \gamma_+ \gamma_-} \tag{1}$$

where $W_{n,0}$ is the rate of the generation of electron−hole pairs at some high-energy state n, γ_{nn} is the energy relaxation rate of state n, ξ_{1n} is the nonradiative relaxation rate from state n to state 1 due to the thermal interaction with a bath, $V_{0,1}$ and $V_{0,2}$ are the matrix elements of the radiative optical transitions from states 1 and 2 to the ground state 0 of the QD, and ξ_{01} and ξ_{02} are the total dephasing rates of these transitions. The rest of parameters in

eq 1 are defined as follows:

$$\gamma_{\pm} = \frac{1}{2}\left(\gamma_{11} + \gamma_{22} \pm \sqrt{(\gamma_{11} - \gamma_{22})^2 + 4\xi_{21}^2 \exp(-\Delta E/k_B T)}\right) \quad (2)$$

where $\gamma_{11} = \xi_{01} + \xi_{21}$ and $\gamma_{22} = \xi_{02} + \xi_{21}\exp(-\Delta E/k_B T)$.

Since the ratio of the peak intensities of components PL1 and PL2 depends on the energy gap ΔE, we can use the steady-state luminescence spectra corresponding to the QDs of different sizes to estimate the unknown parameters entering eq 1. This ratio is of the form

$$C(x) = \frac{S_{PL2}}{S_{PL1}} = \frac{A\xi_{21}}{\xi_{02} + \xi_{21}\exp(-x)}$$

where $A = (|V_{0,2}|^2\xi_{01})/(|V_{0,1}|^2\xi_{02})$ and $x = \Delta E/k_B T$. By measuring the value of C for different x, we may find A and relate the rates ξ_{21} and ξ_{02}. The quantitative analysis of the experimental size dependencies of the PL1 and PL2 intensities is rather difficult, due to the strong overlapping of the corresponding spectral bands. Nevertheless, the calculation of $C(x)$ gave close results for several pairs of the QD diameters 3.8, 4, 4.4, and 5.5 nm. The most reliable values, $C(3.96) = 3.05$ and $C(1.9) = 0.68$, were obtained for the QDs of diameters 4 and 4.9 nm, respectively, whose PL spectra are shown in Figure 2b. Using this data, we obtain

$$\xi_{21} = \frac{C(x_1) - C(x_2)}{C(x_2)e^{-x_2} - C(x_1)e^{-x_1}}\xi_{02} \quad (3a)$$

$$A = C(x_1)C(x_2)\frac{e^{-x_2} - e^{-x_1}}{C(x_1) - C(x_2)} \quad (3b)$$

The relaxation constant ξ_{02} will be found from the size dependency of the PL decay time.

Using the proposed model, it is easy to show that the decay of components PL1 and PL2 for $t \gg t_0$, where t_0 is the excitation pulse duration, may be described by the expressions

$$G_{PL1}(t) = ae^{-t/\tau_+} + be^{-t/\tau_-} \quad (4a)$$

$$G_{PL2}(t) = ce^{-t/\tau_+} + de^{-t/\tau_-} \quad (4b)$$

where $\tau_{\pm} = 1/\gamma_{\pm}$, and a, b, c, and d are some time-independent coefficients. It is seen that PL1 and PL2 components manifest biexponential decay, with the exponentials characterized by the shot (τ_+) and long (τ_-) decay times. Hence, the size dependencies of the decay times of components PL1 and PL2 at a given temperature T are predominantly controlled by the size dependence of ΔE (see eq 2).

In our time-resolved experiments, two luminescence bands (PL1 and PL2) were detected for all QD samples. However, the employed experimental setup allowed us to measure PL decay times not faster than 40 ns, so that the signals of the fast components of bands PL1 and PL2 manifest themselves in Figure 3a in the form of small spikes about the origin; the duration of the spikes is close to the width of the temporal instrument function of the experimental setup. It should be borne in mind, therefore, that the experimentally measured decay curves and characteristic times in Figure 3 correspond to the slow components of bands PL1 and PL2.

According to eq 2, the decay times are $\tau_+ = 1/\gamma_{11}$ and $\tau_- = 1/\xi_{02}$ for $x \gg 1$. This fact allows one to find $\xi_{02} \approx 4 \times 10^5\ s^{-1}$ from the measured value of the PL decay time, which is 2.5 μs for the QDs with diameter 3.7 nm and $x \approx 11.46$. Using this value in eq 3, we obtain $A \approx 0.11$ and $\xi_{21} \approx 2.18 \times 10^7\ s^{-1}$.

Numerical estimation shows that, typically, $\tau_+ < 46$ ns, since the upper limit of the short relaxation time equals $1/\xi_{21}$. The experimental setup used for the transient photoluminescence experiments enabled us to measure the PL decay with characteristic times above 20 ns. This feature and the fact that only monoexponential decays in the microsecond time scale have been observed for the PL signals from all QD samples allow us to assign these signals to the slow exponentials of components PL1 and PL2 described by the second terms in eq 4, with the characteristic time $\tau_- = 1/\gamma_-$.

Figure 4b shows the comparison between the experimentally measured PL decay time (solid squares) and the time $\tau_- = 1/\gamma_-$ (dashed curve) calculated using eq 2 with $\xi_{21} = 2.18 \times 10^7\ s^{-1}$, $\xi_{01} = 3 \times 10^6\ s^{-1}$, and $\xi_{02} = 4 \times 10^5\ s^{-1}$. The employed values of the relaxation constants were chosen to provide the best fit to the experimental data. The experimental data are seen to be in good agreement with the analytical results everywhere, except for the region $x < 0.42$, where a sharp reduction of the luminescence decay time is observed. This discrepancy between the experimental and theoretical data indicates the presence of an additional mechanism of energy relaxation. This fact is not surprising, since the employed relaxation model does not take into account the dependency of the relaxation parameters ξ_{01}, ξ_{02}, and ξ_{21} on ΔE. It is quite obvious that when ΔE varies in the broad range from 300 to 5 meV, different types of relaxation mechanisms with a threshold-like behavior may contribute to the relaxation process. For example, when ΔE approaches from above the value $n\hbar\Omega$, where n is the integer and $\hbar\Omega$ is the optical-phonon energy, the mechanism involving n optical phonons start to facilitate the energy relaxation. It is quite probable that this mechanism is responsible for the step-like structure of the experimental dependency of the PL decay time on ΔE in Figure 4b (see the region $1 \le x < 5$).

For $x < 1$, mechanisms involving acoustic phonons may start to dominate the energy relaxation.[36−38] This fact can be demonstrated using a simple model of the luminescence decay time $\tau_- = 1/\gamma_-$, which is most sensitive to the variation of ξ_{01} in the region $x < 1$. Suppose that $\xi_{01}(\Delta E) = \xi_{01} + \xi_{01}^{ac}/\{1 + \exp[-p(\Delta E_0 - \Delta E)]\}$, where ξ_{01}^{ac} is the acoustic-phonon-induced

relaxation rate, ΔE_0 is the peak energy in the acoustic-phonon density of states, and the factor $1/\{1 + \exp[-p(\Delta E_0 - \Delta E)]\}$ reduces to the Heaviside step function as $p \rightarrow \infty$. The red curve in Figure 4b shows the results of the calculation of the decay time τ_- for the following set of parameters (found from the best fit of the experimental data): $\Delta E_0 = 5.2$ meV, $p = 10$ meV^{-1}, and $\xi_{01}^{ac} = 2 \times 10^7$ s^{-1}. It is seen that the theoretical curve quantitatively agrees with the experimental data in the entire region of ΔE. It is quite remarkable that the employed value of ΔE_0 is close to the energies of acoustic phonons TA(X), LA(X), and TA(L) of PbS.[39]

CONCLUSIONS

The electronic energy structure and dynamics of low-energy optical transitions in PbS QDs in tetrachloroethylene have been studied for the broad range of the QD sizes from 2.3 to 8.8 nm, which corresponds to the emission range from 0.65 to 1.8 eV. Two bands with the size-dependent relative intensities were found in the steady-state luminescence spectra of the QDs. One of them, with the Stokes shift of ~5 meV, was attributed to the fundamental optical transition of the QD. Another band, whose size-dependent Stokes shift decreases with the QD's size, was attributed—in accordance with the previous reports[19,20,22,23]—to the electron state with the size-dependent energy within the QD's bandgap.

A 10-fold reduction in the lowest-energy luminescence decay time with the QD size was found for PbS QDs at room temperature. Such a reduction has never been reported for semiconductor QDs before, to the best of our knowledge. The observed dependency was explained in terms of the phonon-induced transitions from the in-gap state to the fundamental state of QDs, which become essential when the energy gap between the two states is comparable to, or less than, the thermal energy k_BT. The steady-state and transient luminescence from QDs of different sizes was described in the framework of a simple model of optical transitions, whose predictions were shown to be in good agreement with the experimental data. The origin of the in-gap state is still an open issue. The fact that the size dependency of the in-gap state's energy, as observed by us, is almost twice as weak as that of the similar dependency of the QD's fundamental transition is a strong argument in support of the model proposed by Fernée *et al.*,[20] which assumes that the energy of only one particle constituting the electron–hole pair is size-quantized. The revealed deviation of the size dependency from the one expected in the case where the energies of both particles are dependent on the QD size, may also be due to the difference in the effective masses of electrons (holes) in PbS QDs and in the bulk material, as it was observed for CdS QDs in the strong confinement regime.[40] The origin of the in-gap state and the dominant relaxation mechanisms warrant further investigation, which requires experimental studies with higher spectral and time resolutions.

METHODS

Synthesis and Characterization of PbS Quantum Dots. PbO (>99.9%), oleic acid (90%), 1-octadecene (90%), hexamethyldisilthiane, and TCM (>99.5%, for IR spectroscopy) were purchased from Aldrich and used without further purification. The PbS QDs were synthesized in the three-neck, 25-ml flask equipped with a magnetic stirrer and adapters for vacuum drying, argon flow, and precursors injection. One mmol of PbO, 4 mmol of oleic acid, and 10 mL of octadecene were loaded into the flask. The reaction mixture was heated up to 170 °C and dried under the 10-mbar vacuum for 30 min, until all of the reagents have completely dissolved and formed a clear solution. Further, 0.2 mmol of hexamethyldisilathiane in 0.5 mL of octadecene was injected into the mixture at 100 °C, under the argon flow and intense stirring. The reaction mixture was additionally stirred for 1–15 min at 70°–100 °C, in order to grow PbS nanocrystals (QDs) of the desired diameters (ranging from 2.5 to 8.8 nm) and to get the edge of the absorption band between 800 and 1900 nm. The reaction mixture was then cooled down to 50–60 °C, and the QDs were deposited using isopropyl alcohol. Finally, the QDs were centrifuged for 5 min at a speed of 6000 rpm, washed twice with isopropyl alcohol, and redispersed in TCM.

The thus obtained QDs were optically characterized at room temperature using NIR absorption spectroscopy and quasi-state and transient NIR luminescence spectroscopy, while their size and composition were determined with X-ray diffraction (Ultima IV, Rigaku) and scanning transmission electron microscopy (Merlin, Zeiss, STEM mode). The absorption spectra of PbS-QDs/TCM were measured using a UV-3600 Shimadzu spectrophotometer.

The steady-state photoluminescence was analyzed with a home-built setup.[41,42] The luminescence was detected using a Hamamatsu G5852–21 InGaAs photodiode cooled to −20 °C, with the sensitivity spectral range of 0.9–2.1 μm. The 10^{-6} M of PbS-QDs/TCM placed in a 3×3 mm^2 quartz cell was excited by a 633-nm laser beam. The luminescence was collected in 90° geometry and sent through an Acton SP-2558 monochromator, with a relative aperture of 6:5, a focal length of 0.5 m, and the diffraction grating with a period of 150 mm^{-1} (the wavelength resolution in the 0.9–2.1 μm spectral range was about 6 nm). The spectral sensitivity of the setup was determined using a blackbody emission spectrum, and then used to normalize the luminescence spectra. The PL quantum yield was determined by employing the standard procedure[43] and using IR-1061TM (Sigma-Aldrich) organic dye with the quantum yield of 1.7% as a reference standard.

For the luminescence decay studies, an experimental setup analogous to that described in the work by Parfenov *et al.*[44] was used. The luminescence from PbS-QDs/TCM was excited by 100-ps pulses of a PicoQuant LDH-P-C-640B laser, emitting at 640-nm wavelength and producing 0.4-nJ pulses at 60-Hz repetition rate. The power density of the excitation light on the sample was about 20 μW/cm^2, in order to avoid any photobleaching of QDs during the time-resolved experiments. The signal of luminescence was first sent through the relevant band-selective filter, with a bandpass 100–150 nm, and then focused on a 0.1-mm^2 detector area. A fast Femto HCA-S-200M-IN detector based on an InGaAs pin-photodiode and a Stanford Research SR455A amplifier enabled measurements in the spectral range from 0.8 to 2.0 μm and in the time interval from 20 ns to 10 μs. A high-frequency digital oscilloscope Tektronix

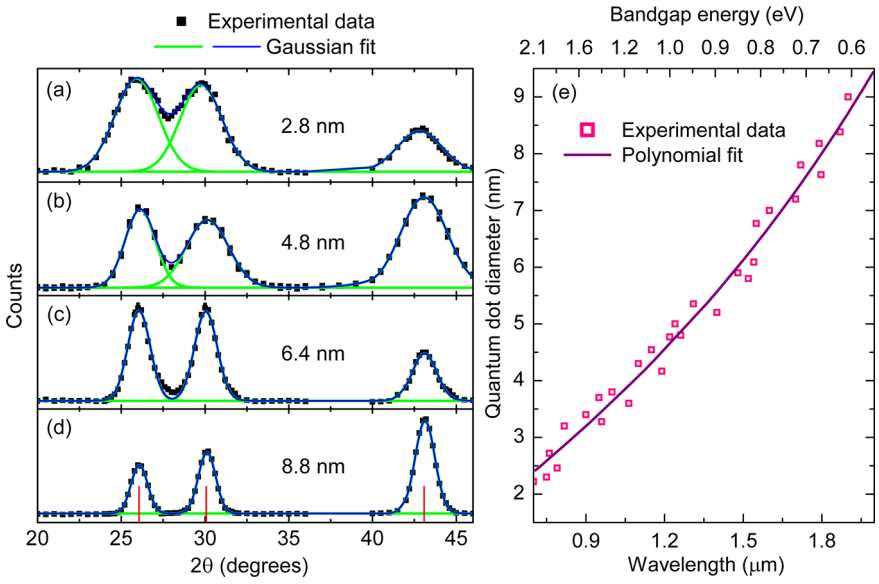

Figure 5. (a−d) Typical powder XRD patterns for PbS QDs of different mean diameters (determined from the FWHM of the XRD peaks). The patterns, fitted by three Gaussians each (green curves), demonstrate that the QDs' crystal structure corresponds to that of the bulk PbS (vertical lines show the positions of the corresponding peaks in the bulk material). (e) Wavelengths (bottom axis) and energies (top axis) of the fundamental absorption bands in PbS QDs of different mean diameters. The experimental data shown by open squares is fitted with the polynomial function in eq 5.

TDS-2002 (with a 200-MHz bandpass and a 2-GHz sampling frequency), performing an average over 128 measurements, was used. A computer program, purpose-built for additional accumulation of up to 10^6 measurements, read signals from the oscilloscope. The time needed to record a single luminescence decay curve with the use of this program was about 1 h.

A representative set of room-temperature absorption and PL spectra of the synthesized PbS QDs of different sizes, with the energy of the lowest absorption band within the range of 0.65−1.8 eV, are shown in Figure 1. It is of significance that the PL quantum yield did not manifest noticeable size dependence and was about 30% for the four PbS-QDs/TCM samples, with the QDs' mean diameters of 3, 4, 4.9, and 8 nm.

Figure 5 panels a−d show the typical powder X-ray diffraction (XRD) patterns for PbS QDs of different diameters. The figures confirm the chemical composition and crystal structure of the synthesized QDs, since the positions of the diffraction peaks are approximately equal to those expected for bulk PbS with a rock-salt structure and a lattice constant of 0.5936 nm.[45] The diffraction peaks are seen to broaden when the QDs' size is reduced. This effect stems from the finite size of the crystallites and their structural defects. The mean diameter D of the QDs was calculated using the Scherrer formula[46]

$$D = \frac{k\lambda}{\Delta(2\theta)\cos\theta}$$

where λ is the wavelength of the X-rays, $\Delta(2\theta)$ is the full width at half-maximum (FWHM) of the XRD peak corresponding to the Bragg angle 2θ, and $k = 1$. To determine the FWHM of the XRD peaks, the measured diffraction patterns were fitted with three Gaussians each and the FWHM was calculated as an arithmetical mean over the three XRD peaks. The calculations show that the mean diameters of the synthesized QDs lie in the range from 2.5 to 8.8 nm, while the positions of the lowest-energy absorption peak change from 1.77 to 0.65 eV. For the samples characterized by $D = 4.8$, 6.4, and 8.8 nm, the sizes of the QDs were also determined using the scanning transmission electron microscopy (STEM). The samples were prepared by dipping a carbon-coated microscopy grid in a diluted QD solution. The mean QD diameters of 4.9 ± 0.3, 6.6 ± 0.2, and 9.0 ± 0.2 nm were obtained from the analysis of the STEM images (not shown). A good agreement between the XRD and STEM data indicates a good crystalline structure of the synthesized QDs.

The size dependence of the wavelength of the first excitonic absorption band of PbS-QDs/TCM is shown in Figure 5b. Following the work by Yu *et al.*,[15] the experimental data were fitted using the empirical polynomial

$$D(\lambda) = 7.2 \times 10^{-10}\lambda^3 - 1.7 \times 10^{-6}\lambda^2 + 5.7 \times 10^{-3}\lambda - 0.9 \quad (5)$$

where D (nm) is the mean diameter of QDs in a given nanocrystal sample and λ (nm) is the wavelength of the lowest-energy absorption peak of the sample. This polynomial allows one to determine D directly from the absorption measurements, while avoiding conduction of either STEM or XRD analysis for each sample synthesized. The dependency $D(\lambda)$ agrees to a precision of 5% with that found from the empirical formula $E_{BG} = 0.41 + 100/[D(2.52D + 28.3)]$ (E_{BG} is in eV), which was proposed by Moreels *et al.*[18] The results presented in this section show that the chemical composition, crystal structure, and size-dependent optical properties of the synthesized PbS QDs do not significantly differ from those reported by other authors,[19−24] who also studied the electronic energy structure and dynamics of low-energy optical transitions in PbS QDs dispersed in liquid solutions. The comparison of spectral widths of the lowest-energy absorption peaks for the QDs of different sizes with the data in the available literature, and the estimation of the width of the QD size distribution using eq 5, showed that the QD size dispersion did not exceed 12%.

Conflict of Interest: The authors declare no competing financial interest.

Acknowledgment. This work was supported by the Russian Foundation for Basic Research (Grants Nos 12-02-01263 and 12-02-00938) and the Ministry of Education and Science of the Russian Federation (Projects Nos 11.519.11.3020, 11.519.11.3026, and 14.740.11.1366). M.A. and A.V.P. acknowledge financial support from the Belarussian CHEMREAGENTS program. The work of I.D.R. was supported by the Australian Research Council, through its Discovery Early Career Researcher Award DE120100055.

REFERENCES AND NOTES

1. Ma, Q.; Su, X. Near-Infrared Quantum Dots: Synthesis, Functionalization and Analytical Applications. *Analyst* **2010**, *135*, 1867–1877.

2. Rogach, A. L.; Eychmüller, A.; Hickey, S. G.; Kershaw, S. V. Infrared-Emitting Colloidal Nanocrystals: Synthesis, Assembly, Spectroscopy, and Applications. *Small* **2007**, *3*, 536–557.
3. Kang, I.; Wise, F. W. Electronic Structure and Optical Properties of PbS and PbSe Quantum Dots. *J. Opt. Soc. Am. B* **1997**, *14*, 1632–1646.
4. Yu, W.; Falkner, J.; Shih, B.; Colvin, V. Preparation and Characterization of Monodisperse PbSe Semiconductor Nanocrystals in a Noncoordinating Solvent. *Chem. Mater.* **2004**, *16*, 3318–3322.
5. Hyun, B. R.; Chen, H. Y.; Rey, D. A.; Wise, F. W.; Batt, C. A. Near-Infrared Fluorescence Imaging with Water-Soluble Lead Salt Quantum Dots. *J. Phys. Chem. B* **2007**, *111*, 5726–5730.
6. Konstantatos, G.; Howard, I.; Fischer, A.; Hoogland, S.; Clifford, J.; Klem, E.; Levina, L.; Sargent, E. H. Ultrasensitive Solution-Cast Quantum Dot Photodetectors. *Nature* **2006**, *442*, 180–183.
7. Steckel, J. S.; Coe-Sullivan, S.; Bulovic, V.; Bawendi, M. G. 1.3 μm to 1.55 μm Tunable Electroluminescence from PbSe Quantum Dots Embedded within an Organic Device. *Adv. Mater.* **2003**, *15*, 1862–1866.
8. Bakueva, L.; Musikhin, S.; Hines, M. A.; Chang, T.-W. F.; Tzolov, M.; Scholes, G. D.; Sargent, E. H. Size-Tunable Infrared (1000−1600 nm) Electroluminescence from PbS Quantum-Dot Nanocrystals in a Semiconducting Polymer. *Appl. Phys. Lett.* **2003**, *82*, 2895–2897.
9. Schaller, R.; Klimov, V. High Efficiency Carrier Multiplication in PbSe Nanocrystals: Implications for Solar Energy Conversion. *Phys. Rev. Lett.* **2004**, *92*, 186601.
10. McDonald, S. A.; Konstantatos, G.; Zhang, S.; Cyr, P. W.; Klem, E. J. D.; Levina, L.; Sargent, E. H. Solution-Processed PbS Quantum Dot Infrared Photodetectors and Photovoltaics. *Nat. Mater.* **2005**, *4*, 138–142.
11. Jiang, X.; Schaller, R. D.; Lee, S. B.; Pietryga, J. M.; Klimov, V. I.; Zakhidov, A. A. PbSe Nanocrystal/Conducting Polymer Solar Cells with an Infrared Response to 2 Micron. *J. Mater. Res.* **2007**, *22*, 2204–2210.
12. *Semiconductors, Data Handbook*, 3rd ed.; Madelung, O., Ed.; Springer: New York, 2004.
13. Sapra, S.; Nanda, J.; Pietryga, J. M.; Hollingsworth, J. A.; Sarma, D. D. Unraveling Internal Structures of Highly Luminescent PbSe Nanocrystallites Using Variable-Energy Synchrotron Radiation Photoelectron Spectroscopy. *J. Phys. Chem. B* **2006**, *110*, 15244–15250.
14. Murray, C. B.; Sun, S.; Gaschler, W.; Doyle, H.; Betley, T. A.; Kaganet, C. R. Colloidal Synthesis of Nanocrystals and Nanocrystal Superlattices. *IBM J. Res. Dev.* **2001**, *45*, 47–56.
15. Yu, W. W.; Qu, L.; Guo, W.; Peng, X. Experimental Determination of the Extinction Coefficient of CdTe, CdSe, and CdS Nanocrystals. *Chem. Mater.* **2003**, *15*, 2854–2860.
16. Du, H.; Chen, C. L.; Krishnan, R.; Krauss, T. D.; Harbold, J. M.; Wise, F. W.; Thomas, M. G.; Silcox, J. Optical Properties of Colloidal PbSe Nanocrystals. *Nano Lett.* **2002**, *2*, 1321–1324.
17. Wehrenberg, B. L.; Wang, C. J.; Guyot-Sionnest, P. J. Interband and Intraband Optical Studies of PbSe Colloidal Quantum Dots. *Phys. Chem. B* **2002**, *106*, 10634–10640.
18. Moreels, I.; Lambert, K.; Smeets, D.; De Muynck, D.; Nollet, T.; Martins, J. C.; Vanhaecke, F.; Vantomme, A.; Delerue, C.; Allan, G.; *et al.* Size-Dependent Optical Properties of Colloidal PbS Quantum Dots. *ACS Nano* **2009**, *3*, 3023–3030.
19. Warner, J. H.; Thomsen, E.; Watt, A. R.; Heckenberg, N. R.; Rubinutein-Dunlop, H. Time-Resolved Photoluminescence Spectroscopy of Ligand-Capped PbS Nanocrystals. *Nanotechnology* **2005**, *16*, 175–179.
20. Fernée, M. J.; Thomsen, E.; Jensen, P.; Rubinsztein-Dunlop, H. Luminescence from a Hybrid State Found in Strongly Quantum Confined PbS Nanocrystals. *Nanotechnology* **2006**, *17*, 956–962.
21. Turyanska, L.; Patanè, A.; Henini, M.; Hennequin, B.; Thomas, N. R. Temperature Dependence of the Photoluminescence Emission from Thiol-Capped PbS Quantum Dots. *Appl. Phys. Lett.* **2001**, *90*, 101913.
22. Zhang, J.; Jiang, X. Confinement-Dependent Below-Gap State in PbS Quantum Dot Films Probed by Continuous-Wave Photoinduced Absorption. *J. Phys. Chem. B* **2008**, *112*, 9557–9560.
23. Lewis, J. E.; Wu, S.; Jiang, X. J. Unconventional Gap State of Trapped Exciton in Lead Sulfide Quantum Dots. *Nanotechnology* **2010**, *21*, 455402.
24. Espiau de Lamaëstre, R.; Bernas, H.; Pacifici, D.; Franzò, G.; Priolo, F. Evidence for a "Dark Exciton" State of PbS Nanocrystals in a Silicate. *Appl. Phys. Lett.* **2006**, *88*, 181115.
25. Hyun, B.-R.; Bartnik, A. C.; Lee, J.-K.; Imoto, H.; Sun, L.; Choi, J. J. J.; Chujo, Y.; Hanrath, T.; Ober, C. K.; Wise, F. W. Role of Solvent Dielectric Properties on Charge Transfer from PbS Nanocrystals to Molecules. *Nano Lett.* **2010**, *10*, 318–323.
26. Clark, S. W.; Harbold, J. M.; Wise, F. W. Resonant Energy Transfer in PbS Quantum Dots. *J. Phys. Chem. C* **2007**, *111*, 7302–7305.
27. Curry, R. J. Comment on "Unconventional Gap State of Trapped Exciton in Lead Sulfide Quantum Dots". *Nanotechnology* **2011**, *22*, 238001.
28. Lewis, J. E.; Wu, S.; Jiang, X. Reply to Comment on "Unconventional Gap State of Trapped Exciton in Lead Sulphide Quantum Dots". *Nanotechnology* **2011**, *22*, 238002.
29. An, J. M.; Franceschetti, A.; Zunger, A. Excitonic Exchange Splitting and Radiative Lifetime in PbSe Quantum Dots. *Nano Lett.* **2007**, *7*, 2129–2135.
30. Kim, D.; Kuwabara, T.; Nakayama, M. Photoluminescence Properties Related to Localized States in Colloidal PbS Quantum Dots. *J. Lumin.* **2006**, *119−120*, 214–218.
31. Porteanu, H.; Sirota, M.; Lifshitz, E. Continuous and Time-Resolved Photoluminescence Study of Leads Sulfide Nanocrystals, Embedded in Polymer Film. *J. Cryst. Growth* **1999**, *196*, 126–134.
32. Rinnerbauer, V.; Egelhaaf, H. J.; Hingerl, K.; Werner, S.; Warming, T.; Hoffmann, A.; Kovalenko, M.; Heiss, W.; Hesser, G.; Schaffler, F. Energy Transfer in Close-Packed PbS Nanocrystal Films. *Phys. Rev. B* **2008**, *77*, 085322.
33. Allan, G.; Delerue, C. Confinement Effects in PbSe Quantum Wells and Nanocrystals. *Phys. Rev. B* **2004**, *70*, 245321.
34. *CRC Handbook of Chemistry and Physics*, 68th ed.; Weast, R. C., Ed.; CRC: Boca Raton, FL, 1987.
35. Blum, K. *Density-Matrix Theory and Applications*; Plenum Press: New York, 1981.
36. Kruchinin, S. Yu.; Fedorov, A. V.; Baranov, A. V.; Perova, T. S.; Berwick, K. Resonant Energy Transfer in Quantum Dots: Frequency-Domain Luminescent Spectroscopy. *Phys. Rev. B* **2008**, *78*, 125311.
37. Al Salman, A.; Tortschanoff, A.; Mohamed, M. B.; Tonti, D.; van Mourik, F.; Chergui, M. Temperature Effects on the Spectral Properties of Colloidal CdSe Nanodots, Nanorods, and Tetrapods. *Appl. Phys. Lett.* **2007**, *90*, 093104.
38. Takagahara, T. Theory of Exciton Dephasing in Semiconductor Quantum Dots. *Phys. Rev. B* **1999**, *60*, 2638–2652.
39. Elcombe, M. M. The Crystal Dynamics of Lead Sulphide. *Proc. R. Soc. London* **1967**, *A300*, 210–217.
40. Baranov, A. V.; Inoue, K.; Toba, K.; Yamanaka, A.; Petrov, V. I.; Fedorov, A. V. Resonant Hyper-Raman and Second-Harmonic Scatterings in a CdS Quantum Dot System. *Phys. Rev. B* **1996**, *53*, R1721–R1724.
41. Parfenov, P. S.; Baranov, A. V.; Veniaminov, A. V.; Orlova, A. O. A Complex for the Fluorescence Analysis of Macro- and Microsamples in the Near-Infrared. *J. Opt. Tech.* **2011**, *78*, 120–123.
42. Parfenov, P. S.; Litvin, A. P.; Baranov, A. V.; Veniaminov, A. V.; Ushakova, E. V. Calibration of the Spectral Sensitivity of Instruments for the Near Infrared Region. *J. Appl. Spectrosc.* **2011**, *78*, 433–439.
43. Parker, C. A. *Photoluminescence of Solutions: With Applications to Photochemistry and Analytical Chemistry*; Elsevier Pub. Co.: New York, 1968.
44. Parfenov, P. S.; Litvin, A. P.; Baranov, A. V.; Ushakova, E. V.; Fedorov, A. V.; Prudnikau, A. V.; Artemyev, M. V. Measurement of the Luminescence Decay Times of PbS Quantum

Dots in the Near-IR Spectral Range. *Opt. Spectrosc.* **2012**, *112*, 939–944.
45. Wyckoff, R. W. G. *Crystal Structures*, 2nd ed.; Interscience Publishers: New York, 1963.
46. Cullity, B. D. *Elements of X-Ray Diffraction*; Addison-Wesley: New York, 1977.